HHS Public Access

Author manuscript

Ultrasonics. Author manuscript; available in PMC 2024 July 01.

Published in final edited form as:

Ultrasonics. 2023 July ; 132: 106993. doi:10.1016/j.ultras.2023.106993.

Chronic Effects of Pulsed High Intensity Focused Ultrasound Aided Delivery of Gemcitabine in a Mouse Model of Pancreatic Cancer

Tatiana D. Khokhlova[1], **Yak-Nam Wang**[2], **Helena Son**[1], **Stephanie Totten**[2], **Stella Whang**[1], **Joo Ha Hwang**[3]

[1]Department of Medicine, University of Washington, Seattle, WA 98195, USA

[2]Applied Physics Laboratory, University of Washington, Seattle, WA 98195, USA

[3]Department of Medicine, Stanford University, Palo Alto, CA 98195, USA

Abstract

Pulsed high intensity focused ultrasound (pHIFU) is a non-invasive method that allows to permeabilize pancreatic tumors through inertial cavitation and thereby increase the concentration of systemically administered drug. In this study the tolerability of weekly pHIFU-aided administrations of gemcitabine (gem) and their influence on tumor progression and immune microenvironment were investigated in genetically engineered KrasLSL.G12D/þ; p53R172H/þ; PdxCretg/þ (KPC) mouse model of spontaneously occurring pancreatic tumors. KPC mice were enrolled in the study when the tumor size reached 4–6 mm and treated once a week with either ultrasound-guided pHIFU (1.5 MHz transducer, 1 ms pulses, 1% duty cycle, peak negative pressure 16.5 MPa) followed by administration of gem (n=9), gem only (n=5) or no treatment (n=8). Tumor progression was followed by ultrasound imaging until the study endpoint (tumor size reaching 1 cm), whereupon the excised tumors were analyzed by histology, immunohistochemistry (IHC) and gene expression profiling (Nanostring PanCancer Immune Profiling panel). The pHIFU+gem treatments were well tolerated; the pHIFU-treated region of the tumor turned hypoechoic immediately following treatment in all mice, and this effect persisted throughout the observation period (2–5 weeks) and corresponded to areas of cell death, according to histology and IHC. Enhanced labeling by Granzyme-B was observed within and adjacent to the pHIFU treated area, but not in the non-treated tumor tissue; no difference in CD8+ staining was observed between the treatment groups. Gene expression analysis showed that the pHIFU+gem combination treatment lead to significant downregulation of 162 genes related to immunosuppression, tumorigenesis, and chemoresistance vs gem only treatment.

Correspondence to: Tatiana D. Khokhlova, 300 9th Ave, Seattle, WA 98104, Harborview Medical Center, Research and Training Building, Room 513, tdk7@uw.edu.

Declaration of interests

Tatiana Khokhlova, Joo Ha Hwang reports financial support was provided by National Institutes of Health. Tatiana Khokhlova is an Associate Editor for Ultrasonics - T.K.

Keywords

pulsed HIFU; drug delivery; pancreatic cancer; tumor microenvironment; cavitation

1. Introduction

Pancreatic cancer is one of the deadliest malignancies with very few effective therapeutic options and is the fourth leading cause of cancer-related mortality in the United States [1]. The average 5-year overall survival rate is only 10%, in part because it is difficult to diagnose at an early stage. Although surgery provides a potentially curative treatment, over 80% of patients are diagnosed at advanced, unresectable stage: 35% of those patients have locally advanced disease, and 50% have metastatic disease [2,3]. Systemic chemotherapy is currently the first line treatment for both locally advanced and metastatic pancreatic cancer, with gemcitabine being the standard treatment for over a decade that provided modest survival benefits [4]. More recently, combination chemotherapy with oxaliplatin, irinotecan, fluorouracil, and leucovorin (FOLFIRINOX [FFX]) and gemcitabine (GEM) plus nab-paclitaxel (GnP) was found to be effective, with improved overall survival for patients with metastatic pancreatic cancer and locally advanced [3,5,6]. However, even in those studies the median overall survival rate was no more than 15.5 months for locally advanced disease. This is likely due to the unique tumor microenvironment in pancreatic cancer, comprising extensive stromal desmoplasia and profound infiltration of immunosuppressive cells [7]. Mechanistically, dense stroma and increased intratumoral pressure impede the penetration of systemically administered drugs into the tumor; furthermore, the interactions of cancer cells with the tumor microenvironment components facilitate tumor progression and chemoresistance through a number of mechanisms.

Mechanical effects produced by ultrasound when combined with ultrasound contrast agents (UCAs) have been extensively investigated in recent years for mitigating the mechanistic barriers to chemotherapy – an approach known as sonoporation [8]. In particular, the combination of commercially available UCAs – microbubbles – with chemotherapeutic agents have been used to improve pancreatic ductal adenocarcinoma (PDAC) therapy through sonoporation in both preclinical [9, 10] and clinical studies [11], and retardation of tumor growth and associated improvement in survival have been demonstrated. One of the limiting factors of this approach however, is that UCAs are generally confined to the vasculature and to perivascular space. This limits their access to poorly vascularized regions of the tumor. In addition, sonoporation requires co-administration of the UCAs and the chemotherapeutic agent, and requires comparable circulation time of both, which imposes practical limitations. In recent studies, pulsed high intensity focused ultrasound (pHIFU) without UCAs has been successfully applied for permeabilization of murine pancreatic tumor tissue through the generation of continuous inertial cavitation induced *de novo* throughout the tumor [12–14]. Acutely, the treatment resulted in marked mechanical disruption of the stromal matrix, reduction of glycosaminoglycan and associated water content and improved tumor diffusivity (but, importantly, not perfusion) and yielded an up to 4-fold increase in uptake of doxorubicin in the tumor. Importantly, the studies were performed in an *in vivo* genetically engineered mouse model (*KrasLSLG12D/+*, *Trp53LSL-*

R172H/+, *Cre* or "KPC") of PDAC, which, unlike xenograft or subcutaneous models, closely recapitulates the genetic mutations, clinical symptoms and histopathology found in human pancreatic cancer [15,16]. The efficiency of this pHIFU-based drug delivery did not depend on whether pHIFU treatment was administered prior to or simultaneously with the drug, thus circumventing one of the practical limitations of UCA-based approach. On the other hand, mechanical disruption of tumor tissue previously raised concerns of potential risks of acute pancreatitis due to release of pancreatic enzymes [17]. The first objective of the present work was to investigate the tolerability of repeated weekly pHIFU treatment in combination with systemic administration of a relevant chemotherapeutic drug gemcitabine and its effect on tumor progression in KPC mice. The pHIFU-induced enhancement in gemcitabine concentration in the tumor was not quantified in this study. It was expected to be similar if not better than that observed previously for doxorubicin, given that its molecular weight is twice lower.

In addition to alterations of the tumor mechanical properties, the acute mechanical cellular damage resulting from pHIFU-induced cavitation has been shown to stimulate tumor-specific immune response through in situ release of intracellular tumor antigens, danger associated molecular patterns (DAMPs), and pro-inflammatory cytokines in several preclinical tumor models, including PDAC [18–23]. Thus, the second objective of this study was to evaluate the changes to the tumor microenvironment resulting from repeated administration of combined pHIFU-gemcitabine treatments.

2. Materials and Methods

2.1 Experimental design

All animal studies were approved by the Institutional Animal Care and Use Committee of the University of Washington. Genetic PDAC mouse model $Kras^{LSL\text{-}G12D/+}$, $Trp53^{LSL\text{-}R172H/+}$, *Cre* (KPC) was used. KPC animals conditionally express endogenous mutant *Kras* and point mutant *Trp53* alleles, spontaneously develop PDAC and closely mimic the pathophysiology and molecular progression of the human disease [15]. The mice were kept under pathogen-free conditions and received food and water ad libitum. The study timeline is illustrated in Fig.1a; KPC mice were closely monitored and imaged by high resolution diagnostic ultrasound (L7–18 linear array, center frequency 12 MHz, Alpinion Medical Systems, Seoul, Korea) to screen for pancreatic tumor development; when the tumor size reached 4–6 mm according to diagnostic ultrasound examination (at 16–34 weeks of age), the animal was enrolled in the study. The enrolled animals were randomly assigned to either of the three arms of the study: pHIFU treatment immediately followed by gemcitabine (gem) administration (n=9), gem administration only (n=5) or no treatment (n=8). Gem was injected intraperitoneally, at the dose of 100 mg/kg – the maximum dose known to be tolerated by mice [24]. The intratumoral concentrations of gemcitabine were not quantified in the current study, partially due to the absence of a reliable measurement method. The reliability of liquid chromatogtraphy-based measurements of gemcitabine metabolites - active diphosphate and triphosphate –- is controversial. The predictive value of alternative biomarkers of response to gemcitabine therapy (expression of Human Equilibrative Nucleoside Transporter-1, hENT-1, being the most promising one) has been

called into question in large clinical studies [25]. Further, as mentioned previously, the changes in gemcitabine uptake induced by pHIFU treatment were expected to be similar to those observed previously for doxorubicin in the acute setting given the similarity in molecular weights [12].

The mice received the treatment weekly, and the tumor dimensions and pHIFU treated area evolution were monitored twice weekly by high resolution ultrasound imaging. For the duration of the study the mice were monitored twice weekly, and their weight and body condition score (BCS) were recorded [26]. When the mice reached at least one of the endpoint criteria of this study – largest tumor dimension reaching 1 cm, BCS less than 2, and gaining or losing over 10% body weight – the mice were euthanized and the necropsy was performed.

2.2 pHIFU treatment

Prior to each pHIFU treatment the study animal was anesthetized by inhalation of isoflurane, and the abdomen was thoroughly shaved and depilated. Thereafter the animal was placed on a water-circulating heating pad maintained at 37°C and onto the treatment bench of the pHIFU system illustrated in Fig.1b. High-resolution ultrasound imaging was performed to precisely measure the dimensions of the tumor and to identify the acoustic window appropriate for the pHIFU treatment. Specifically, gas-filled intestinal loops and stomach typically surrounding the tumor are highly reflective to ultrasound and can prevent the HIFU waves from reaching the focus. In addition, pHIFU exposure of these organs carries a high risk of mechanical damage in mice and human patients alike. In our experiments the acoustic window was maximized by manipulating the mouse position (e.g. mouse on its back or on its side) and, where possible, compressing the bowel loops on top of the tumor by the HIFU coupling balloon. Note that these maneuvers did not always allow acoustic access to the entirety of the tumor; the areas of the tumor obstructed by bowel were not targeted.

The treatment head mounted onto a 3D positioning system included a spherically focused 1.5 MHz HIFU transducer (64 mm aperture, 45 mm focal distance), a ring-shaped focused PCD element (frequency band 3.5–11 MHz) and an US imaging probe (FUL7–18, Alpinion) within the 22 mm central opening. The treatment head was coupled to the animal's abdomen through a layer of degassed US gel and an elastic acoustically transparent membrane filled with degassed deionized water that could be expanded or contracted depending on the desired depth of HIFU focus location relatively to the skin surface. The position of the HIFU focus was pre-registered with the US imaging system and displayed as a yellow cross on the B-mode images. During treatment planning the cross was positioned 2–3 mm below the tumor center to account for the prefocal shift of the cavitation area that we previously observed with this system (Fig.1c). This shift was likely due to HIFU beam refraction at the boundary between the coupling balloon filled with room temperature water (sound speed 1,480 m/s) and mouse body (estimated sound speed 1,580 m/s).

To generate the pHIFU treatment grid in the two transverse dimensions the treatment head was moved in cranio-caudal direction in 1 mm steps, and treatment areas were defined within each plane with 1 mm spacing. The pHIFU treatment was then initiated, during which the treatment head was moved in a raster pattern along the planned grid,

and delivering the same pHIFU exposure at each spot: 60 pulses of 1 ms duration, pulse repetition frequency (PRF) of 1 Hz, output power set to 400 W. This output level corresponded to a highly nonlinear pressure waveform at the focus, with peak positive pressure of 82 MPa, and peak negative pressure of 16.5 MPa, as measured with fiber optic probe hydrophone (FOPH2000, RP Acoustics, Leutenbach, Germany). This output level was used in our prior experiments to generate consistent inertial cavitation activity with every pulse, per PCD detection of broadband noise emissions, which was confirmed here [12]. Cavitation activity was occasionally observed in the prefocal region on US imaging as a faint and transient hyperechoic region (Supplemental Video 1 and Fig.1c), consistently with our prior studies that used this pHIFU regime [27]. Of note, this appearance of cavitation is markedly different from bright and persistent hyperechoic regions that form during histotripsy and/or boiling histotripsy treatments [22,27].

2.3 Histology and immunohistochemistry

At the endpoint the tumor was dissected and embedded in optimum cutting temperature medium and frozen in isopentane cooled on dry ice. Embedded tissue was stored at −80°C until sectioning. Serial 4-μm sections were taken from the frozen-embedded tumors and stained with Masson's Trichrome (MT) to visualize tissue structure and collagen distribution, or used for the following immunohistochemistry (IHC) markers: apoptosis marker caspase-3 (CC3, Cell Signaling, Cat. No 9579, dilution 1:250), proliferation marker Ki67 (Cell Signaling, Cat. No 12202, 1:400), CD8 (BD Pharmingen, Cat. No 550281, 1:400), and Granzyme B (Abcam, Cat. No ab4059, 1:100). Before staining endogenous enzyme block and protein block were applied to avoid non-specific binding, and appropriate staining controls have been performed. The numbers of cells stained positive for CC3 and Ki67 were manually counted within $n=9$ windows 400×800 μm in size randomly positioned over the slide and averaged. The numbers of cells stained positive for CD8 were counted using the same method, but the window sizes were larger (1.5×2.5 mm), and the windows were randomly positioned over the tumor core or the tumor periphery (n=5 each).

2.4 Gene expression analysis

An additional 50-μm section of each tumor was used for mRNA extraction (Absolutely RNA miniprep kit, Cat. No. 400800, Agilent, Santa Clara, CA) and gene expression analysis with Nanostring nCounter PanCancer Immune Profiling Panel (Nanostring Inc, Seattle, WA), which contains 770 genes involved in cancer immune response and include 19 housekeeping genes for data normalization. Read counts from the raw data output were assessed for differential gene expression after normalization using NanoString nSolver (version 4.0). Immune cell type scoring in nSolver was used to assess relative abundance of tumor infiltrating leukocytes. This method of characterizing immune cell populations was previously validated against IHC and flow cytometry [28]. The results were plotted using Prism GraphPad (San Diego, CA).

2.5 Statistical analysis

Two-sided Student's t-test was used to evaluate pairwise differences between groups in the relative tumor volumes at each time point, and numbers of CC3+ and Ki67+ cells in IHC slides. Differential gene expression in pHIFU+gem vs gem, and gem vs control group was

analyzed using Nanostring nSolver 4.0, and presented in the form of volcano plots (log2 fold change vs log10 *P*-value). A *P* value of less than 0.05 was deemed significant in all analyses; no correction for multiple comparisons was made.

3. Results

3.1 Treatment tolerability, tumor growth dynamics and ultrasound imaging features

Both treatments – pHIFU+gem and gem alone – were generally well tolerated, with none of the mice requiring analgesia after treatment and exhibiting no outward signs of pain. No deterioration in BCS, significant changes in body weight (weight variations were 1.7±1.9% of the weight at enrollment across the groups) or behavioral patterns were noted in any of the animals over the duration of the study before the endpoint criterion of the tumor being 1 cm in the largest dimension was reached. In pHIFU+gem group the majority of the animals (n=6) received two treatments before the endpoint, n=1 animal received one treatment; in n=2 animals the tumors became completely acoustically inaccessible after one and three pHIFU+gem treatments, and therefore received one and two gem only treatments, respectively, before reaching the endpoint criterion.

On necropsy, no distant metastases in the liver or lung were observed in any animals. The tumor growth curves for the two treatment groups, and no treatment control group are shown in Fig.2a.

Both treatments resulted in significant retardation of tumor growth compared to the no treatment control group, but the tumor growth dynamics were not different between gem only and pHIFU+gem groups. A trend towards retardation of tumor growth in the pHIFU+gem group was only seen after day 14, and by then most animals in that group had already reached the endpoint (maximum tumor size of 1 cm) except one that reached it on day 35. Immediately following treatment, the area of the tumor treated with pHIFU appeared slightly to moderately hypoechoic relatively to the pre-treatment images and adjacent unaffected tumor border (Fig.2b).

This was consistent with our prior observations of pHIFU acute effects [12,14], and was previously hypothesized to result from partial loss of stromal integrity, and breaking down of hyaluronan water complexes and increasing the concentration of free fluid. The presence of this hypoechogenicity persisted for at least a week, until next pHIFU treatment, and for up to 3 weeks in the case where the tumor became acoustically inaccessible (Fig.2c). Notably, the sizes of these treated hypoechoic regions did not change appreciably within the observation period, whereas the adjacent untreated tumor areas continued to grow. No consistent changes in echogenicity were observed for gem only treatment group or control group.

3.2 Effect of treatment on tumor structure, viability and proliferation

Figure 3 illustrates the effects of pHIFU+gem (a-c) and gem only (d-f) treatments on tumor structure (per MT stain), viability (per CC3 stain) and proliferation (per Ki67 stain). Both the cellular and the stromal structures within the central pHIFU-treated region outlined with a dotted yellow line are significantly disrupted, as seen in the overall, low magnification MT-stained section of the tumor. The higher magnification images show a nearly complete

loss of cellular structure within the more glandular areas of the tumor (b) and disoriented, frayed and separated collagen bundles in the more stromal areas (c). Vascular structures within the treated areas were similarly disrupted. This is in contrast with immediate acute effects of pHIFU observed in our prior studies, where viable tumor cells were still present within the disrupted area [12].

Bright positive CC3 staining at the border of and inside the pHIFU treated region, taken together with paucity of Ki67-positive staining indicate that cells are not proliferating and are undergoing cell death. Conversely, outside of the pHIFU-treated region the expression pattern is reversed: fewer CC3-positive cells and more Ki67-positive cells are observed. The tumors in gem-treated group (d) were generally less differentiated at the core (e) and more differentiated at the periphery (f), but contained only occasional small pockets of necrosis (e.g. one seen in (e)). Few cells positive for CC3 could only be seen at and immediately adjacent to those areas, whereas Ki67-positive cells were uniformly distributed throughout the tumor, similarly to what was observed for the tumor areas not affected by pHIFU treatment. Indeed, per IHC quantitation shown in Fig.3g, the number of Ki-67 positive cells was not significantly different for the tumors in the two treatment groups, but the number of CC3-positive cells was significantly higher in pHIFU+gem group.

3.3 Effect of treatment on tumor-infiltrating CD8+ T cells

Figure 4 shows representative serial tumor sections stained for CD8 and Granzyme B for the experimental groups. In all samples, CD8+ T cells were seen in well differentiated, peripheral areas of the tumors in similar numbers in gem only and pHIFU+gem groups, and lower numbers in control group, but not at the less differentiated tumor core and/or within pHIFU-treated region. Presence of these cells corresponded to very faint if any Granzyme B staining, which indicated lack of function and/or exhaustion. Conversely, areas of intense Granzyme-B-positive staining, both diffuse and focal, were present within pHIFU-treated regions without corresponding CD8+ staining. These areas were consistent with enhanced CC3 staining, as granzyme B is known to promote CC3-dependent cell death [30]. The absence of co-localization of CD8+ and granzyme B staining suggested either the participation of tumor infiltrating lymphocytes other than CD8+ T cells, e.g. NK/NKT or CD4+ T cells, or enhanced presence of granzyme B in the extracellular space, potentially due to mechanical rupture of extracellular matrix (ECM) and myeloid derived suppressor cells (MDSCs) that are known to contain it [31,32]. Given the absence of differential expression of GzB mRNA in pHIFU-treated tumors, per gene expression analysis presented below, the latter explanation appears to be more likely.

3.3 Effect of treatment on tumor microenvironment

The differential gene expression in the tumors from gem only vs no treatment control, pHIFU+gem vs gem only, and pHIFU+gem vs control are shown in Fig.5 as volcano plots. Gem only treatment resulted in only minor changes in gene expression profile relative to control receiving no treatment – 6 genes were significantly downregulated and 33 significantly upregulated out of 770 genes on the panel (see Supplementary Table S1). Many of the differentially expressed genes with known roles in the context of pancreatic cancer corresponded to immunosuppression, tumorigenesis, and chemoresistance,

as illustrated in Figs.6a,b. Conversely, pHIFU+gem treatment had a larger effect on gene expression in the tumors: 161 genes were significantly differentially expressed relatively to gem only treatment, and primarily downregulated (149 genes). Interestingly, many of the genes upregulated in gem vs control group were downregulated in pHIFU+gem group by approximately the same amount or more (Fig.6a). Other subsets of genes, known specifically in the context of pancreatic cancer to promote immunosuppression, tumor-supporting complement system and inflammation, as well as chemoresistance are summarized in Fig.6c [40–57]. Many of the downregulated genes correspond to signaling pathways that have been targets of inhibition by immunotherapies in clinical trials, in particular *PDL1*, *CD19*, *CCl5-CCR5* axis, *Il6st* and *CD39* [41–45].

The results of cell type scoring analysis were only conclusive for changes in abundance of T cells and B cells, but not for cytotoxic cells, dendritic cells, macrophages, neutrophils, NK cells and exhausted T cells (Supplementary Fig.S2). Specifically, the nSolver quality control p-values indicating the validity of each cell type's measurement (i.e. genes previously shown to be characteristic of cell population) were $p<0.001$ for T cells and $p<0.01$ for B cells. The abundance of both cell types increased in gem only vs control group, and decreased in pHIFU+gem vs gem alone. This was consistent with observations from IHC staining for CD8+ cells (Fig.4): administration of gemcitabine alone increased their frequency in well differentiated areas of the tumor vs control, whereas pHIFU+gem decreased the overall volume of viable cells in the tumor, including the CD8+ cells. Further, the trends for other cell types –B cells, cytotoxic cells and exhausted CD8 cells were similar, and changes in macrophages and DCs were less pronounced.

4. Discussion

In this study the effects of weekly pHIFU treatments followed by the administration of gemcitabine, on tumor progression, structure and microenvironment were evaluated in KPC mice. While pHIFU+gem treatments did not appear to reduce the overall tumor volume compared to gem only group within the observation period, it substantially reduced the viable tumor volume. Specifically, the persistently hypoechoic area treated with pHIFU corresponded on histology to dead or dying cells, disrupted stromal matrix and vasculature, whereas the adjacent peripheral areas of the tumor, unaffected by pHIFU continued to grow. Although the areas disrupted and necrotized by pHIFU can be expected to contract and resolve over time, it could take 2–4 weeks for this process to begin, according to prior studies of pHIFU mechanical ablation in small animals [59, 60]. This was outside of the observation period in the current study - 2 weeks in the majority of subjects due to the choice of endpoint criterion (1 cm tumor size). Further, it was not possible to definitively conclude whether this necrotizing effect was due to pHIFU cavitation effects only - toxic extracellular milieu from lysed cells, stroma and proteoglycans, disruption of vasculature and anoxia - or their combination with cytotoxicity of gem promoted by its enhanced diffusion through permeabilized tissue. Those questions will be addressed in future studies.

The pHIFU apparatus and exposures used here were optimized specifically for treating very small, millimeter-sized tumors without affecting adjacent vital organs that are also very sensitive due to their small size. In particular, the HIFU transducer was very highly focused

and operated at the frequency of 1.5 MHz, both to keep the focal area small. The use of this transducer design for human use is impractical, as the treatment of the entire tumor volume would take too long. Thus, a clinically relevant pHIFU transducer should ideally have a larger focal area, that could be achieved by reducing the focusing angle and the frequency, while providing the same level of inertial cavitation under the same pulsing regime as used here. This was recently shown to be feasible: the same cavitation level was achieved at lower peak negative pressures (5.5 MPa vs 13 MPa) with less focused transducers (F-number of 1.5 vs 0.77) and at slightly lower frequency (1 MHz vs 1.5 MHz), while the focal area was over 16-fold larger [63]. Additional increase in treatment rate could be achieved by increasing the pulse repetition frequency while keeping the duty factor for each treatment location low by rapid electronic steering of the pHIFU beam with a multi-element array.

Cavitation-induced mechanical effects on different tumors have previously been shown to induce inflammatory response, and promote T-cell mediated anti-tumor immunity[19–24, 59–61]. Most notably, in a recent study the effects of a combination treatment with pHIFU-induced cavitation and immune checkpoint inhibitors (anti PD-1 and CTLA-4) on tumor progression, and number and function of infiltrating lymphocytes were evaluated in an orthotopically grafted KPC pancreatic tumor [19]. The pHIFU exposure used in that study was applied once, and used lower power and longer pulses (200W vs 400W, and 10 ms vs 1 ms) than the current study. The induced mechanical disruption effects on the tumor were less drastic (petechial hemorrhage acutely, and reduced cell density in 12 days) and confined to smaller areas of the tumors. The infiltration of the tumor by CD8+ T cells per IHC staining in both pHIFU alone and pHIFU with checkpoint inhibition groups were approximately doubled relative to controls at 12 day time point. Conversely, in current study CD8+ T cells were found to infiltrate only well differentiated areas at the tumor periphery in similar numbers in both pHIFU+gem and gem only groups, and were not co-located with granzyme-B positive staining, which indicated their lack of functionality and exhaustion. These results were confirmed by cell type scoring based on gene expression profiling. Paucity of infiltrating CD8+ T cells in the more advanced, poorly differentiated tumors in KPC mice is well documented in literature [62]. Their absence in pHIFU-treated areas may potentially be explained by increased cytotoxicity there, both from direct release of a large volume of intracellular products into the extracellular space due to cavitation-based disruption of cells, and/or from larger concentration of gemcitabine due to enhanced diffusivity[14]. Repeated pHIFU treatments would also contribute to killing of any lymphocytes, including CD8+, that may infiltrate the treated region the week prior.

Gene expression profiling of the tumors indicated that pHIFU+gem treatment induced broad changes to the tumor microenvironment relatively to gem only treatment, that overall corresponded to less immunosuppressive and tumorigenic milieu. Downregulated gene subsets implicated in tumor chemoresistance appear to be particularly important in the context of enhancing the effect of gemcitabine. Pancreatic tumors are known to develop resistance to cytotoxicity of within weeks of treatment initiation, and several metabolic mechanisms have been implicated in this process: disruption of internalization and activation of the drug inside the tumor cells that are necessary to induce cell death, entrapment of the drug within cancer associated fibroblasts (CAFs) and pancreatic stellate cells (PSCs), thus decreasing its bioavailability [58]. *Tap1* regulates transporter associated with antigen

processing I, involved in chemoresistance, downstream of hedgehog signaling [51]; *Bcl2* regulates Beclin2, which regulates apoptosis and promotes resistance to drug-induced cytotoxicity [54]; *Itch* is a signaling pathway that promotes metastatic growth, and its inhibition was shown to sensitize cells to gemcitabine [55]; *Fap* (fibroblast activation protein) is expressed by cancer-associated fibroblasts, overexpressed in all PDAC, and is associated with poor survival [53]. It is responsible for desmoplastic reaction, supports building of blood vessels, and is also immunosuppressive. Toll like receptor 8 (*Tlr8*) is known to regulate carcinogenesis and promote tumor growth [56].

Of the few gene sets that were significantly upregulated in pHIFU+gem group, *Pparγ*, should be pointed out as it is an important promoter of M2 polarization of macrophages, and could be involved in activation of MDSCs [7]. *Msln* (mesothelin) is a differentiation antigen and plays an important role in cancer development, especially at an early stage. This is consistent with histological observations that the viable tumor areas in pHIFU+gem group are more differentiated. Mesothelin is extensively expressed in pancreatic cancer, and has been a target of a number of clinical and preclinical trials of antibody-based therapies [41], suggesting a potential for a combination treatment with pHIFU+gem. Further, many of the downregulated genes corresponded to targets of immunotherapies previously used in clinical trials in patients with pancreatic cancer. Those changes most likely corresponded to the peripheral, well differentiated and better perfused areas of the tumor, given the paucity of viable cells in the pHIFU-treated core. Thus, the viable areas of the tumor may be expected to be more amenable to additional systemically administered therapeutics, including immunotherapies. In particular, the combination of anti-PD1 and anti-CTLA4 with pHIFU was shown in the previous study to confer survival benefit in an orthotopic KPC mouse model [19].

The main limitation of this study was that it did not include a pHIFU only treatment group, and it was thus impossible to differentiate the tumoricidal effects of pHIFU-induced cavitation from those induced by enhanced penetration of gemcitabine. This is due, in part, to the original premise of pHIFU treatment as a strategy to enhance chemotherapy rather than an independent therapy. With addition of pHIFU only treatment group, a more in-depth investigation of cells deemed responsible for microenvironment changes observed here – primarily tumor associated macrophages and MDSCs – is warranted via flow cytometry and IHC.

To conclude, in this work we demonstrated that repeated pHIFU-aided gemcitabine administration is well tolerated in KPC mice with pancreatic tumors, and has extensive tumoricidal effect. In addition, pHIFU+gem treatment disrupts important immunosuppressive signaling pathways in the tumor microenvironment, and sensitizes the tumor to gemcitabine.

Supplementary Material

Refer to Web version on PubMed Central for supplementary material.

Acknowledgements:

We would like to thank the University of Washington Histology and Imaging Core for performing immunohistochemistry staining reported in this work, Cassie Sather and Genomics Resource at Fred Hutchinson Cancer Research Center for running the Nanostring panels and advice on sample preparation, and Ms. Kayla Gravelle for her role in maintaining the KPC mouse colony.

Funding:

This work was funded by the National Cancer Institute [grant number R01 CA154451] and Donald E. Bocek endowed development award in Pancreatic Cancer.

References

1. Available online: Cancer stats 2021: https://acsjournals.onlinelibrary.wiley.com/doi/epdf/10.3322/caac.21654
2. Kamarajah SK; Burns WR; Frankel T.Ll; Cho CS;, Nathan H Validation of the American Joint Commission on Cancer (AJCC) 8th Edition Staging System for Patients with Pancreatic Adenocarcinoma: A Surveillance, Epidemiology and End Results (SEER) Analysis. Ann Surg Oncol. 2017, 24(7), 2023–2030. [PubMed: 28213792]
3. Arima S; Kawahira M; Shimokawa M; Ido A; Koga F; Ueda Y; Nakazawa J; Komori A; Otsu S; Fukahori M; Makiyama A; Taguchi H; Honda T; Shibuki T; Mitsugi K; Nio K; Ide Y; Ureshino N; Mizuta T,; Shirakawa T; Otsuka T; Gemcitabine Plus Nab-Paclitaxel Versus FOLFIRINOX in Locally Advanced, Unresectable Pancreatic Cancer: A Multicenter Observational Study (NAPOLEON Study). Pancreas. 2021, 50(7), 957–964. [PubMed: 34347735]
4. Burris HA 3rd; Moore MJ; Andersen J; Green MR; Rothenberg ML; Modiano MR; Cripps MC; Portenoy RK; Storniolo AM; Tarassoff P; Nelson R; Dorr FA; Stephens CD; Von Hoff DD Improvements in survival and clinical benefit with gemcitabine as first-line therapy for patients with advanced pancreas cancer: a randomized trial. J Clin Oncol. 1997, 15(6), 2403–13. [PubMed: 9196156]
5. Conroy T, Desseigne F, Ychou M, Bouché O, Guimbaud R, Bécouarn Y, Adenis A, Raoul JL, Gourgou-Bourgade S, de la Fouchardière C, Bennouna J, Bachet JB, Khemissa-Akouz F, Péré-Vergé D, Delbaldo C, Assenat E, Chauffert B, Michel P, Montoto-Grillot C, Ducreux M. FOLFIRINOX versus gemcitabine for metastatic pancreatic cancer. N Engl J Med. 2011 364(19), 1817–25. [PubMed: 21561347]
6. Von Hoff DD, Ervin T, Arena FP, Chiorean EG, Infante J, Moore M, Seay T, Tjulandin SA, Ma WW, Saleh MN, Harris M, Reni M, Dowden S, Laheru D, Bahary N, Ramanathan RK, Tabernero J, Hidalgo M, Goldstein D, Van Cutsem E, … Renschler MF Increased survival in pancreatic cancer with nab-paclitaxel plus gemcitabine. N Engl J Med, 2013, 369(18), 1691–1703. [PubMed: 24131140]
7. Liu Q; Liao Q; Zhao Y Chemotherapy and tumor microenvironment of pancreatic cancer. Cancer Cell Int, 2017, 17, 68. [PubMed: 28694739]
8. Chowdhury SM, Abou-Elkacem L, Lee T, Dahl J, Lutz AM Ultrasound and microbubble mediated therapeutic delivery: Underlying mechanisms and future outlook. 2020, J. Control Release, 326, 75–90. [PubMed: 32554041]
9. Kotopoulis S, Delalande A, Popa M, Mamaeva V, Dimcevski G, Gilja OH, Postema M, Gjertsen BT, McCormack E Sonoporation-enhanced chemotherapy significantly reduces primary tumour burden in an orthotopic pancreatic cancer xenograft. Mol Imaging Biol, 2014, 16(1), 53–62. [PubMed: 23877869]
10. Bressand D, Novell A, Girault A, Raoul W, Fromont-Hankard G, Escoffre JM, Lecomte T, Bouakaz A Enhancing Nab-Paclitaxel Delivery Using Microbubble-Assisted Ultrasound in a Pancreatic Cancer Model. Mol. Pharmaceutics, 2019, 16(9), 3814–3822.
11. Dimcevski G, Kotopoulis S, Bjånes T, Hoem D, Schjøtt J, Gjertsen BT, Biermann M, Molven A, Sorbye H, McCormack E, Postema M, Gilja OH A human clinical trial using ultrasound and microbubbles to enhance gemcitabine treatment of inoperable pancreatic cancer. J. Control Release, 2016, 243, 172–181. [PubMed: 27744037]

12. Li T, Wang YN; Khokhlova TD; D'Andrea S; Starr F; Chen H; McCune JS; Risler LJ; Mashadi-Hossein A; Hwang JH. Pulsed High-Intensity Focused Ultrasound Enhances Delivery of Doxorubicin in a Preclinical Model of Pancreatic Cancer. Cancer Res., 2015, 75(18), 3738–46. [PubMed: 26216548]

13. Park EJ; Ahn YD;. Lee JY In vivo study of enhanced chemotherapy combined with ultrasound image-guided focused ultrasound (USgFUS) treatment for pancreatic cancer in a xenograft mouse model. European radiology, 2018, 28(9), 3710–3718. [PubMed: 29600477]

14. Maloney E, Wang YN, Vohra R, Son H, Whang S, Khokhlova T, Park J, Gravelle K, Totten S, Hwang JH, Lee D Magnetic resonance imaging biomarkers for pulsed focused ultrasound treatment of pancreatic ductal adenocarcinoma. World J. Gastroenterol, 2020, 26(9), 904–917. [PubMed: 32206002]

15. Hingorani SR; Wang L; Multani AS; Combs C; Deramaudt TB; Hruban RH; Rustgi AK; Chang S; Tuveson DA. Trp53R172H and KrasG12D cooperate to promote chromosomal instability and widely metastatic pancreatic ductal adenocarcinoma in mice. Cancer Cell, 2005, 7, 469–483. [PubMed: 15894267]

16. Farr N; Wang Y-N; D'Andrea S; Gravelle KM; Hwang JH; Lee D Noninvasive characterization of pancreatic tumor mouse models using magnetic resonance imaging. 2017 Cancer Med, 6, 1082–1090. [PubMed: 28390098]

17. Hwang JH, Wang YN, Warren C, Upton MP, Starr F, Zhou Y, Mitchell SB. Preclinical in vivo evaluation of an extracorporeal HIFU device for ablation of pancreatic tumors. Ultrasound Med Biol. 2009, 35(6):967–75.

18. Maloney E, Khokhlova T, Pillarisetty VG, Schade GR, Repasky EA, Wang YN, Giuliani L, Primavera M, Hwang JH. Focused ultrasound for immuno-adjuvant treatment of pancreatic cancer: An emerging clinical paradigm in the era of personalized oncotherapy. International reviews of immunology, 2017, 36(6), 338–351. [PubMed: 28961038]

19. Mouratidis P, Costa M, Rivens I, Repasky EE, Ter Haar G. Pulsed focused ultrasound can improve the anti-cancer effects of immune checkpoint inhibitors in murine pancreatic cancer. Journal of the Royal Society, Interface, 2021, 18(180), 20210266. [PubMed: 34229458]

20. Hu Z, Yang XY, Liu Y, Sankin GN, Pua EC, Morse MA, Lyerly HK, Clay TM, Zhong P Investigation of HIFU-induced anti-tumor immunity in a murine tumor model., J Transl Med, 2007, 5, 34. [PubMed: 17625013]

21. Eranki A, Srinivasan P, Ries M, Kim A, Lazarski CA, Rossi CT, Khokhlova TD, Wilson E, Knoblach SM, Sharma KV, Wood BJ, Moonen C, Sandler AD, Kim P High-Intensity Focused Ultrasound (HIFU) Triggers Immune Sensitization of Refractory Murine Neuroblastoma to Checkpoint Inhibitor Therapy., Clin Cancer Res, 2020, 26(5), 1152–1161. [PubMed: 31615935]

22. Schade GR, Wang YN, D'Andrea S, Hwang JH, Liles WC, Khokhlova TD Boiling Histotripsy Ablation of Renal Cell Carcinoma in the Eker Rat Promotes a Systemic Inflammatory Response. Ultrasound Med Biol, 2019, 45(1), 137–147. [PubMed: 30340920]

23. Hendricks-Wenger A, Sereno J, Gannon J, Zeher A, Brock RM, Beitel-White N, Simon A, Davalos RV, Coutermarsh-Ott S, Vlaisavljevich E, Allen IC Histotripsy Ablation Alters the Tumor Microenvironment and Promotes Immune System Activation in a Subcutaneous Model of Pancreatic Cancer. IEEE Trans Ultrason Ferroelectr Freq Control, 2021, 68(9), 2987–3000. [PubMed: 33956631]

24. Yip-Schneider MT; Wu H, Stantz K, Agaram N; Crooks PA; Schmidt CM Dimethylaminoparthenolide and gemcitabine: a survival study using a genetically engineered mouse model of pancreatic cancer. BMC Cancer. 2013, 13:194. [PubMed: 23590467]

25. Randazzo O, Papini F, Mantini G, Gregori A, Parrino B, Liu DSK, Cascioferro S, Carbone D, Peters GJ, Frampton AE, Garajova I, Giovannetti E. "Open Sesame?": Biomarker Status of the Human Equilibrative Nucleoside Transporter-1 and Molecular Mechanisms Influencing its Expression and Activity in the Uptake and Cytotoxicity of Gemcitabine in Pancreatic Cancer. Cancers (Basel). 2020,12(11):3206. [PubMed: 33142664]

26. Ullman-Culleré MH; Foltz CJ Body condition scoring: a rapid and accurate method for assessing health status in mice. Lab Anim Sci, 1999, 49(3), 319–323. [PubMed: 10403450]

27. Chevillet JR; Khokhlova TD; Giraldez MD; Schade GR; Starr F; Wang Y-N; Gallichotte EN; Wang K; Hwang JH; Tewari M Release of Cell-free MicroRNA Tumor Biomarkers into the Blood

Circulation with Pulsed Focused Ultrasound: A Noninvasive, Anatomically Localized, Molecular Liquid Biopsy. Radiology. 2017, 283(1), 158–167. [PubMed: 27802108]

28. Danaher P, Warren S, Dennis L, D'Amico L, White A, Disis ML, Geller MA, Odunsi K, Beechem J, Fling SP. Gene expression markers of Tumor Infiltrating Leukocytes. J Immunother Cancer. 2017, 5:18. [PubMed: 28239471]
29. Vohra R; Wang Y-N, Son H, Totten S, Arora A, Maxwell A, Lee D Non-Invasive Monitoring of Increased Fibrotic Tissue and Hyaluronan Deposition in the Tumor Microenvironment in the Advanced Stages of Pancreatic Ductal Adenocarcinoma. Cancers (Basel). 2022, 14(4): 999. [PubMed: 35205746]
30. Cullen SP, Brunet M, Martin SJ Granzymes in cancer and immunity. Cell Death Differ, 2010, 17(4), 616–623. [PubMed: 20075940]
31. Park S, Anderson NL, Canaria DA, Olson MR Granzyme-Producing CD4 T Cells in Cancer and Autoimmune Disease. ImmunoHorizons, 2021, 5(12), 909–917. [PubMed: 34880104]
32. Tibbs E; Cao X Emerging Canonical and Non-Canonical Roles of Granzyme B in Health and Disease. Cancers (Basel). 2022 14(6), 1436. [PubMed: 35326588]
33. Takeuchi S, Baghdadi M, Tsuchikawa T, Wada H, Nakamura T, Abe H, Nakanishi S, Usui Y, Higuchi K, Takahashi M, Inoko K, Sato S, Takano H, Shichinohe T, Seino K, Hirano S Chemotherapy-Derived Inflammatory Responses Accelerate the Formation of Immunosuppressive Myeloid Cells in the Tissue Microenvironment of Human Pancreatic Cancer. Cancer research, 2015, 75(13), 2629–2640. [PubMed: 25952647]
34. Gunderson AJ, Kaneda MM, Tsujikawa T, Nguyen AV, Affara NI, Ruffell B, Gorjestani S, Liudahl SM, Truitt M, Olson P, Kim G, Hanahan D, Tempero MA, Sheppard B, Irving B, Chang BY, Varner JA, Coussens LM Bruton Tyrosine Kinase-Dependent Immune Cell Cross-talk Drives Pancreas Cancer. Cancer discovery, 2016, 6(3), 270–285. [PubMed: 26715645]
35. Rahim MM, Tu MM, Mahmoud AB, Wight A, Abou-Samra E, Lima PD, Makrigiannis AP Ly49 receptors: innate and adaptive immune paradigms. Front Immunol, 2014, 5, 145. [PubMed: 24765094]
36. Wang MT, Fer N, Galeas J, Collisson EA, Kim SE, Sharib J, McCormick F Blockade of leukemia inhibitory factor as a therapeutic approach to KRAS driven pancreatic cancer. Nat Commun, 2019, 10(1), 3055. [PubMed: 31296870]
37. Storz P Targeting protein kinase C subtypes in pancreatic cancer. Expert Rev Anticancer Ther. 2015;15(4):433–438. [PubMed: 25604078]
38. De Lisle RC, Xu W, Roe BA, Ziemer D. Effects of Muclin (Dmbt1) deficiency on the gastrointestinal system. Am J Physiol Gastrointest Liver Physiol. 2008;294(3):G717–G727. [PubMed: 18202109]
39. Schröder J, Schumacher U, Böckelmann LC Thioredoxin Interacting Protein (TXNIP) Is Differentially Expressed in Human Tumor Samples but Is Absent in Human Tumor Cell Line Xenografts: Implications for Its Use as an Immunosurveillance Marker. Cancers, 2020, 12(10), 3028. [PubMed: 33081035]
40. Shi B, Chu J, Huang T, Wang X, Li Q, Gao Q, Xia Q, Luo S The Scavenger Receptor MARCO Expressed by Tumor-Associated Macrophages Are Highly Associated With Poor Pancreatic Cancer Prognosis. Frontiers in oncology, 2021, 11, 771488. [PubMed: 34778091]
41. Fan JQ, Wang MF, Chen HL, Shang D, Das JK, Song J Current advances and outlooks in immunotherapy for pancreatic ductal adenocarcinoma. Molecular cancer, 2020, 19(1), 32. [PubMed: 32061257]
42. van Duijneveldt G, Griffin M, Putoczki TL. Emerging roles for the IL-6 family of cytokines in pancreatic cancer. Clinical science (London, England : 1979), 2020, 134(16), 2091–2115. [PubMed: 32808663]
43. Nywening TM, Wang-Gillam A, Sanford DE, Belt BA, Panni RZ, Cusworth BM, Toriola AT, Nieman RK, Worley LA, Yano M, Fowler KJ, Lockhart AC, Suresh R, Tan BR, Lim KH, Fields RC, Strasberg SM, Hawkins WG, DeNardo DG, Goedegebuure SP,Linehan DC. Targeting tumour-associated macrophages with CCR2 inhibition in combination with FOLFIRINOX in patients with borderline resectable and locally advanced pancreatic cancer: a single-centre, open-label, dose-

finding, non-randomised, phase 1b trial. The Lancet. Oncology, 2016, 17(5), 651–662. [PubMed: 27055731]

44. Jiao X, Nawab O, Patel T, Kossenkov AV, Halama N, Jaeger D, Pestell RG. Recent Advances Targeting CCR5 for Cancer and Its Role in Immuno-Oncology. Cancer research, 2019, 79(19), 4801–4807. [PubMed: 31292161]
45. Allard D, Allard B, Stagg J. On the mechanism of anti-CD39 immune checkpoint therapy. Journal for immunotherapy of cancer, 2020, 8(1), e000186. [PubMed: 32098829]
46. Zhu Y, Knolhoff BL, Meyer MA, Nywening TM, West BL, Luo J, Wang-Gillam A, Goedegebuure SP, Linehan DC, DeNardo DG CSF1/CSF1R blockade reprograms tumor-infiltrating macrophages and improves response to T-cell checkpoint immunotherapy in pancreatic cancer models. Cancer research, 2014, 74(18), 5057–5069. [PubMed: 25082815]
47. Singh SK, Mishra MK, Eltoum IA, Bae S, Lillard JW Jr, Singh R. CCR5/CCL5 axis interaction promotes migratory and invasiveness of pancreatic cancer cells. Scientific reports, 2018, 8(1), 1323. [PubMed: 29358632]
48. Hussain N, Das D, Pramanik A, Pandey MK, Joshi V, Pramanik KC. Targeting the complement system in pancreatic cancer drug resistance: a novel therapeutic approach. Cancer Drug Resist, 2022, 5, 317–27. [PubMed: 35800364]
49. Bushey RT, Gottlin EB, Campa MJ, Patz EF Jr. Complement factor H protects tumor cell-derived exosomes from complement-dependent lysis and phagocytosis. PloS one, 16(6), 2021, e0252577. [PubMed: 34133431]
50. Gomez-Chou SB, Swidnicka-Siergiejko AK, Badi N, Chavez-Tomar M, Lesinski GB, Bekaii-Saab T, Farren MR, Mace TA, Schmidt C, Liu Y, Deng D, Hwang RF, Zhou L, Moore T, Chatterjee D, Wang H, Leng X, Arlinghaus RB, Logsdon CD, Cruz-Monserrate Z Lipocalin-2 Promotes Pancreatic Ductal Adenocarcinoma by Regulating Inflammation in the Tumor Microenvironment. Cancer research, 2017, 77(10), 2647–2660. [PubMed: 28249896]
51. Xu M, Li L, Liu Z, Jiao Z, Xu P, Kong X, Huang H, Zhang Y. ABCB2 (TAP1) as the downstream target of SHH signaling enhances pancreatic ductal adenocarcinoma drug resistance. Cancer letters, 2013, 333(2), 152–158. [PubMed: 23340176]
52. Garrido G, Schrand B, Rabasa A, Levay A, D'Eramo F, Berezhnoy A, Modi S, Gefen T, Marijt K, Doorduijn E, Dudeja V, van Hall T, Gilboa E. Tumor-targeted silencing of the peptide transporter TAP induces potent antitumor immunity. Nature communications, 2019, 10(1), 3773.
53. Kawase T, Yasui Y, Nishina S, Hara Y, Yanatori I, Tomiyama Y, Nakashima Y, Yoshida K, Kishi F, Nakamura M, Hino K. Fibroblast activation protein-α-expressing fibroblasts promote the progression of pancreatic ductal adenocarcinoma. BMC gastroenterology, 2015, 15, 109. [PubMed: 26330349]
54. Muilenburg DJ, Coates JM, Virudachalam S, Bold RJ. Targeting Bcl-2-mediated cell death as a novel therapy in pancreatic cancer. The Journal of surgical research, 2010, 163(2), 276–281. [PubMed: 20452611]
55. de la Fuente M, Jones MC, Santander-Ortega MJ, Mirenska A, Marimuthu P, Uchegbu I, Schätzlein A (2015). A nano-enabled cancer-specific ITCH RNAi chemotherapy booster for pancreatic cancer. Nanomedicine : nanotechnology, biology, and medicine, 2015, 11(2), 369–377. [PubMed: 25267700]
56. Grimmig T, Matthes N, Hoeland K, Tripathi S, Chandraker A, Grimm M, Moench R, Moll EM, Friess H, Tsaur I, Blaheta RA, Germer CT, Waaga-Gasser AM, Gasser M TLR7 and TLR8 expression increases tumor cell proliferation and promotes chemoresistance in human pancreatic cancer. International journal of oncology, 2015, 47(3), 857–866. [PubMed: 26134824]
57. Marshall LA, Marubayashi S, Jorapur A, Jacobson S, Zibinsky M, Robles O, Hu DX, Jackson JJ, Pookot D, Sanchez J, Brovarney M, Wadsworth A, Chian D, Wustrow D, Kassner PD, Cutler G, Wong B, Brockstedt DG, Talay O. Tumors establish resistance to immunotherapy by regulating Treg recruitment via CCR4. Journal for immunotherapy of cancer, 2020, 8(2), e000764. [PubMed: 33243932]
58. Amrutkar M, Gladhaug IP. Pancreatic Cancer Chemoresistance to Gemcitabine. Cancers, 2017, 9(11), 157. [PubMed: 29144412]

59. Schade GR; Brisbane WG; Whang S; Gravelle K; Wang Y-N, Pillarisetty V; Hwang JH; Liles WC; Khokhlova VA, Bailey MR, Khokhlova TD Boiling histotripsy ablation of renal carcinoma in the Eker rat produces significant changes in the immune system. In Abstracts Book of the 6th International Symposium on Focused Ultrasound, Reston, VA, USA, October 21–25, 2018.

60. Worlikar T, Mendiratta-Lala M, Vlaisavljevich E, Hubbard R, Shi J, Hall TL, Cho CS, Lee FT, Greve J, Xu Z. Effects of Histotripsy on Local Tumor Progression in an in vivo Orthotopic Rodent Liver Tumor Model. BME frontiers, 2020, 9830304. [PubMed: 34327513]

61. Hendricks-Wenger A, Hutchison R, Vlaisavljevich E, Allen IC. Immunological Effects of Histotripsy for Cancer Therapy. Frontiers in oncology, 11, 2021, 681629. [PubMed: 34136405]

62. Clark CE, Hingorani SR, Mick R, Combs C, Tuveson DA, Vonderheide RH (2007). Dynamics of the immune reaction to pancreatic cancer from inception to invasion. Cancer research, 2007, 67(19), 9518–9527. [PubMed: 17909062]

63. Bawiec CR, Rosnitskiy PB, Peek AT, Maxwell AD, Kreider W, Haar GRT, Sapozhnikov OA, Khokhlova VA, Khokhlova TD. Inertial Cavitation Behaviors Induced by Nonlinear Focused Ultrasound Pulses. IEEE Trans Ultrason Ferroelectr Freq Control, 2021, 68(9), 2884–2895. [PubMed: 33861702]

Highlights.

- Inertial cavitation was induced in KPC mouse pancreatic tumors by pulsed HIFU (pHIFU)
- Tumors turned persistently hypoechoic on ultrasound imaging post pHIFU treatment
- Weekly combined pHIFU+gemcitabine treatment was well tolerated, had tumoricidal effect
- pHIFU+gemcitabine treatment downregulated tumor immunosuppression and chemoresistance

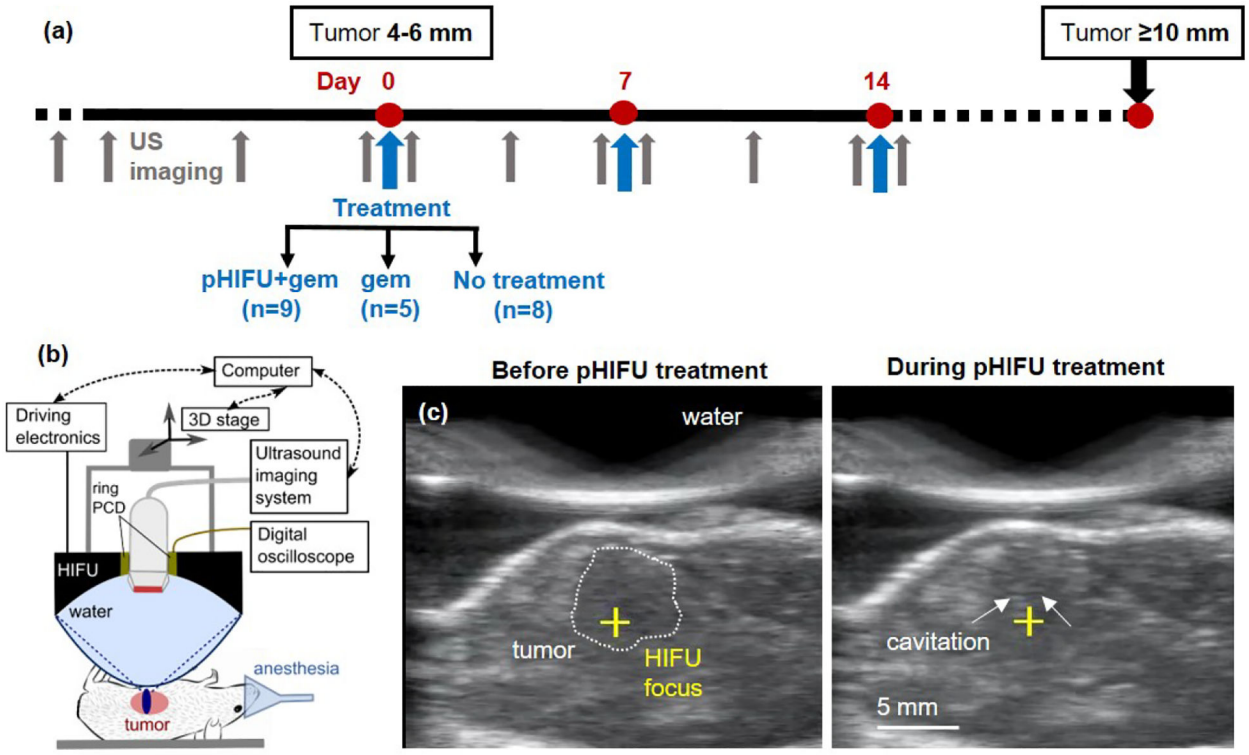

Figure 1.

The study timeline and pHIFU methods. (a) Mice were enrolled when the tumor reached 4–6 mm in size, per US imaging, and treated weekly until tumor size reached 10 mm – the study endpoint. Mice were randomly assigned to three groups: pHIFU followed by IP administration of gemcitabine (gem), gem only or no treatment. (b) Experimental setup for pHIFU treatment of KPC mouse tumors (Alpinion VIFU 2000 dry system). (c) B-mode ultrasound (US) images from the inline probe obtained immediately prior to (left) and during (right) pHIFU treatment. Note the faint hyperechoic region (arrows) appearing prefocally and corresponding to inertial cavitation (see also Supplemental Video 1).

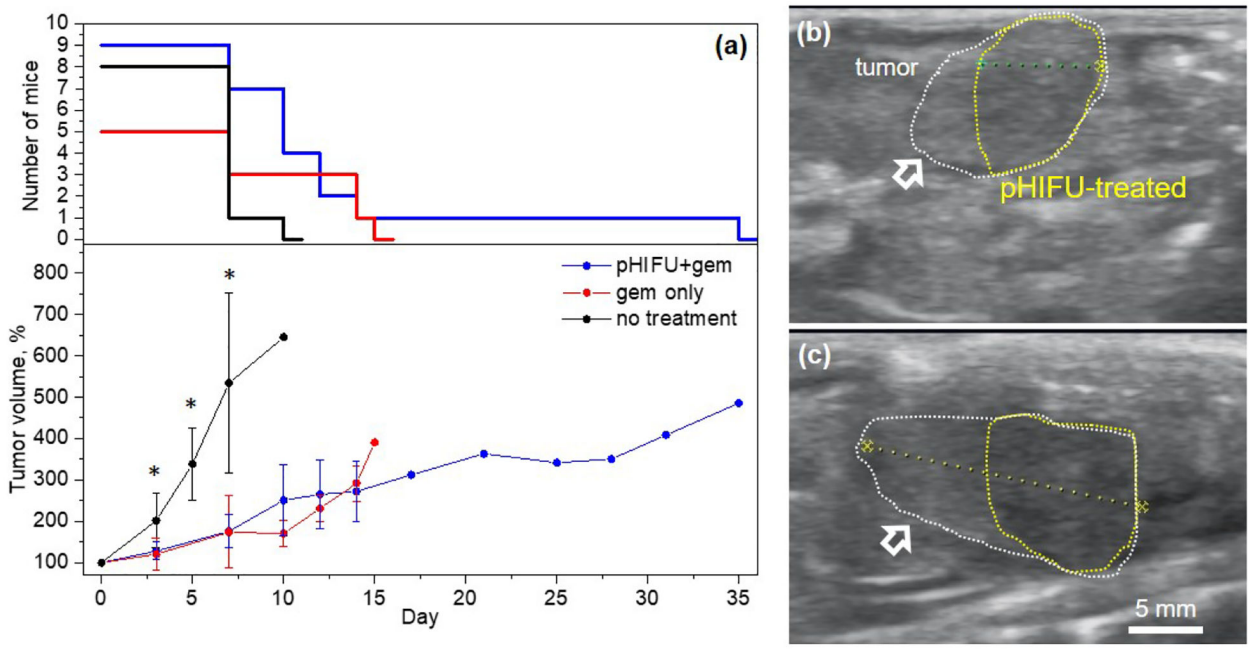

Figure 2.

(a) Tumor growth curves for the three experimental groups; error bars correspond to standard deviation; upper graph indicates the number of mice in each group at each time point. Tumor sizes in both treatment groups are significantly smaller than those in the no treatment control group at 3–7 day time points (*$p < 0.05$) The difference between the tumor sizes in the treatment groups is not statistically significant at any time point in the observation period, and a trend towards tumor growth retardation in pHIFU+gem group is only observed after day 14, which also coincided with the endpoint for most mice in that group. **(b),(c)** Representative US B-mode images of a tumor (white dotted line) treated with pHIFU immediately after and 21 days after treatment, respectively. Note that pHIFU was only applied to acoustically accessible areas of the tumor (yellow dotted line) not obstructed by bowel gas. The pHIFU-treated area consistently appeared slightly hypoechoic throughout the observation period and did not appreciably change in size, whereas the untreated area of the tumor (white arrows) continued to grow.

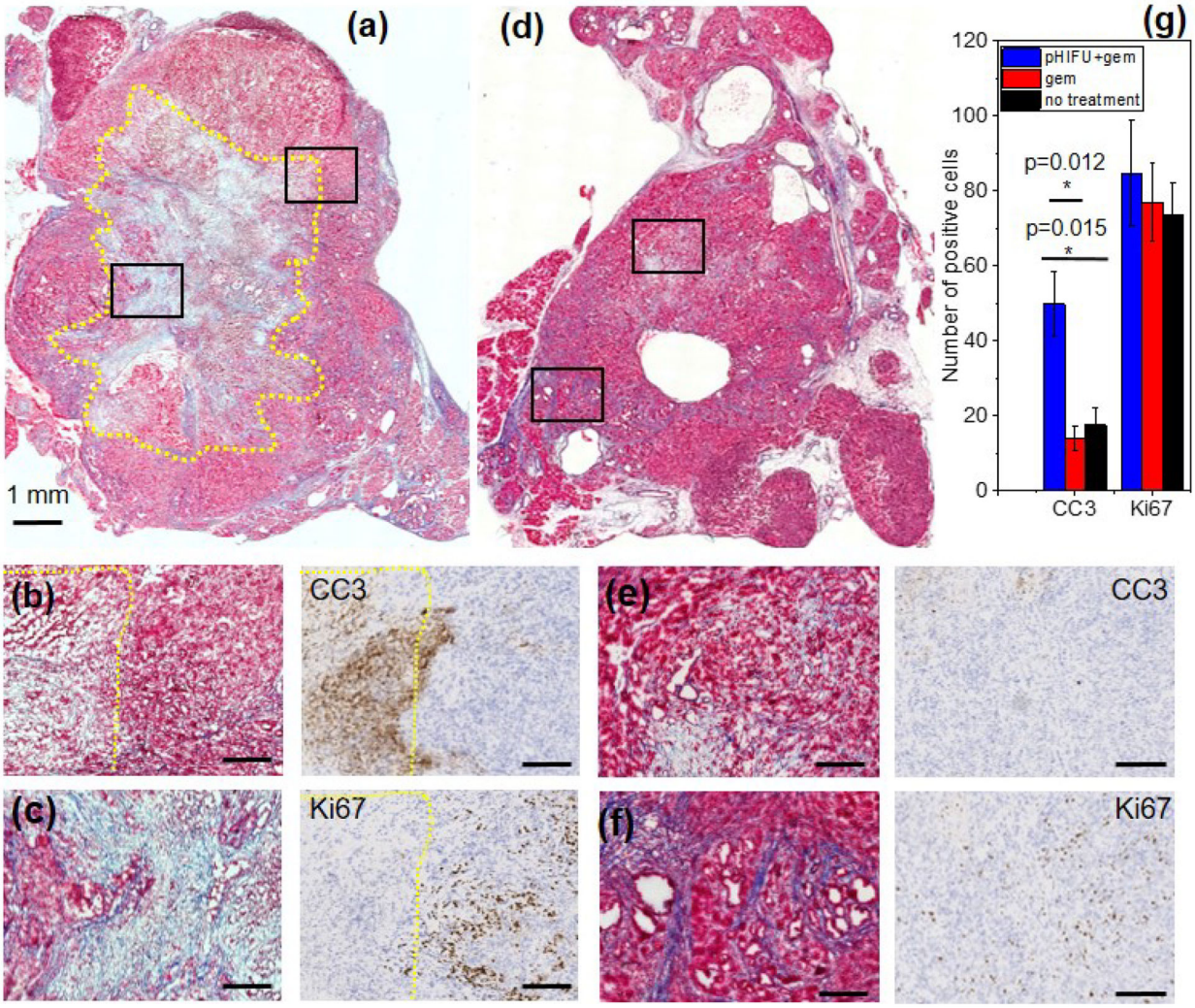

Figure 3.

(a) Representative serial histological sections stained with Masson's Trichrome (MT), caspase-3 (CC3) and Ki67 of a tumor from pHIFU +gem (**(a), (b) (c)**) and gem only (**(d), (e) (f)**) treatment groups**. (a)** The pHIFU-treated region is outlined with yellow dotted line, and is mostly necrotic, with loss of cell structure, fragmented cells and areas of disrupted collagen fibers. Higher magnification images correspond to the black frames in **(a)** and show the more glandular **(b)** and more fibrous **(c)** areas of the tumor. IHC images corresponding to **(b)** show bright positive CC3 staining at the border and inside of the treated region, and no Ki67-positive staining, indicating that cells are damaged beyond repair. Conversely, the surrounding untreated tumor tissue contains few CC3-positive cells, but fairly uniform Ki67-positive staining**. (d)** Low magnification image shows the typical heterogeneity of KPC tumor structure, with glandular areas with occasional small regions of necrosis (higher magnification image in **(e)**) and more fibrous areas (higher magnification image in **(f)**). IHC images corresponding to **(e)** show occasional CC3-positive staining at and surrounding the areas of necrosis, as well as uniform Ki67-positive staining outside of those areas comparable to that in the periphery of pHIFU-treated tumor. Scale bar in all

high magnification images is 250 μm). MT and IHC images for no treatment group were similar to those in gem only group (Supplementary Fig.S1). **(g)** IHC quantification (error bars represent standard error) showing no difference in Ki-67-positive staining between the experimental groups, and significantly larger number of CC3-stained cells in pHIFU-treated tumors.

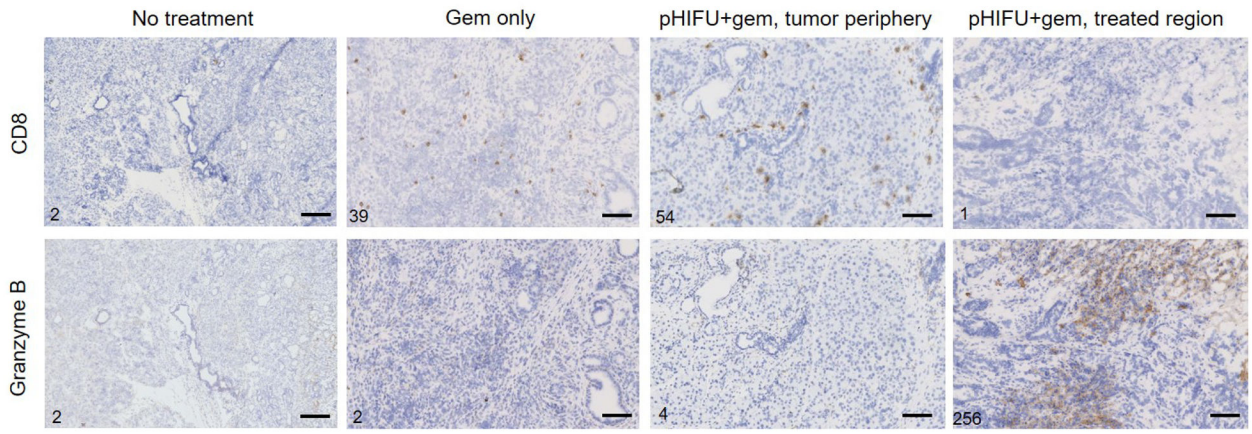

Figure 4.

Serial CD8 and Granzyme B stained sections of tumors from the experimental groups. The numbers of positive cells seen within each frame are provided in the lower left corner of the frame. CD8-positive cells were present in similar numbers in well differentiated, peripheral areas of tumors from both treatment groups, and lower numbers in control group, but with little to no Granzyme-B-positive staining, and were absent from less differentiated areas, the tumor core and pHIFU-treated regions. Conversely, pHIFU-treated regions consistently had intense Granzyme-B-positive staining, with a mixture of diffuse and focal staining that could indicate the presence and activation of immune cells other than CD8+ T cells in those areas. The scale bar in all images is 250 μm.

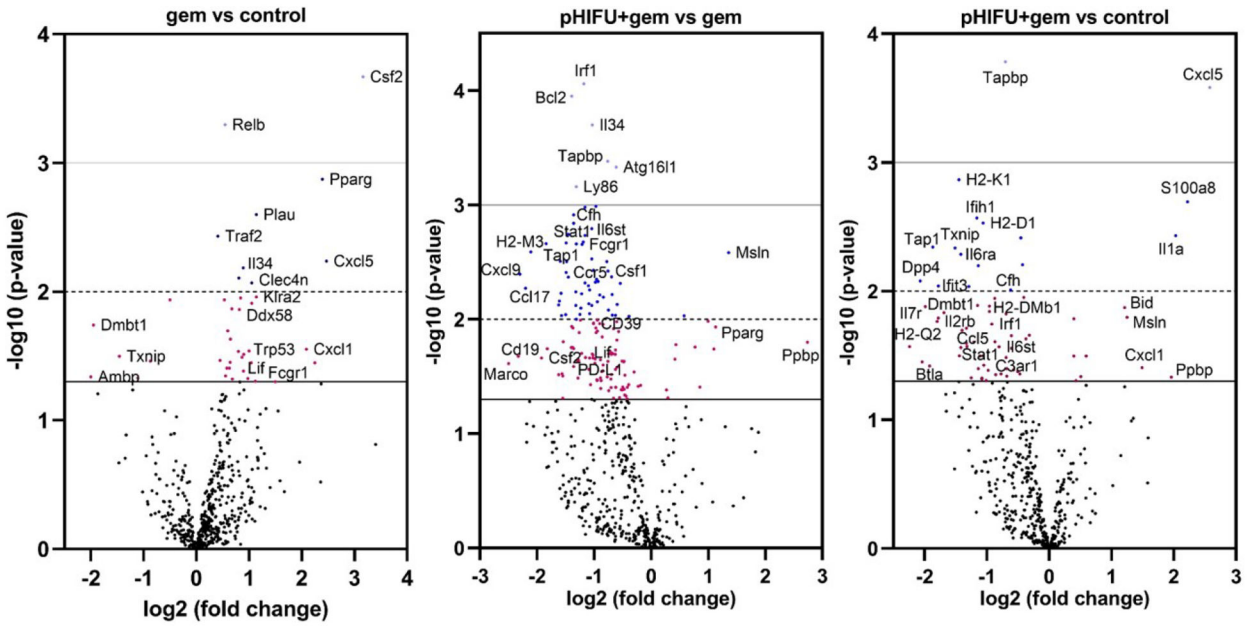

Figure 5.

Overview of differential gene expression in KPC tumors from no treatment control (n=8), gem only (n=5) and pHIFU+gem (n=9) groups. Total RNA was isolated from the tumors and immune profiling performed using the Nanostring PanCancer Immune panel. Of 770 genes the expression of 39 genes was significantly different ($p < 0.05$) in gem only vs control group, and mostly related to upregulation of cancer-supporting immunosuppressive pathways, chemoresistance and tumorigenesis. Conversely, the majority of the 162 genes differentially expressed in pHIFU+gem vs gem only group were downregulated, and related to tumor-supporting complement pathways, chemoresistance and immunosuppression. Differential expression in pHIFU+gem vs control group thus represents a mixture of the two effects described above, with downregulation being dominant (60 out of 71 genes). Thus, pHIFU treatment appears to partially reverse immunosuppression, disrupt tumorigenic and complement pathways, and sensitize the tumors cells to chemotherapy.

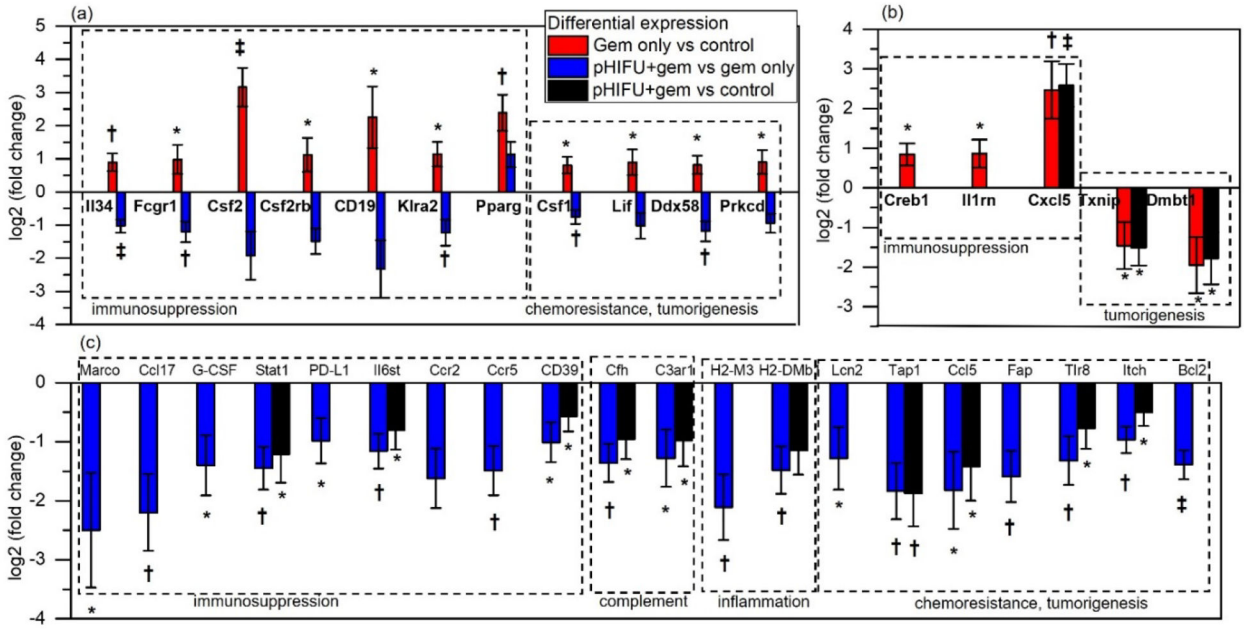

Figure 6.

Differential expression of subsets of genes with known roles in the context of pancreatic cancer [7, 41–42, 44–48, 50–55] that is statistically significant in **(a)** both gem vs control and in pHIFU+gem vs gem, **(b)** only gem vs control, and **(c)** only in pHIFU+gem vs gem. Differential expression of pHIFU+gem vs control is shown for comparison where statistically significant. Most genes that are upregulated by administration of gem alone are downregulated by pHIFU, with a notable exception of PPARγ. Broadly, upregulation of these genes is associated with immunosuppression through attraction of MDSCs and tumor-associated macrophages, tumor-supporting complement system and inflammation, and chemoresistance and tumorigenesis. *$p<0.05$; $^{\dagger}p<0.01$; $^{\ddagger}p<0.001$